ACS Photonics

Article

Cite This: ACS Photonics 2019, 6, 1656−1663

pubs.acs.org/journal/apchd5

Dephasing Free Photon Entanglement with a Quantum Dot

A. Fognini,[†,⊥] A. Ahmadi,[*,‡,⊥] M. Zeeshan,[¶] J. T. Fokkens,[†] S. J. Gibson,[¶] N. Sherlekar,[¶] S. J. Daley,[¶] D. Dalacu,[§] P. J. Poole,[§] K. D. Jöns,[∥] V. Zwiller,[∥,†] and M. E. Reimer[¶]

[†]Kavli Institute of Nanoscience Delft, Delft University of Technology, Delft 2628 CJ, The Netherlands

[‡]Institute for Quantum Computing and Department of Physics and Astronomy, University of Waterloo, Waterloo, Ontario N2L 3G1, Canada

[¶]Institute for Quantum Computing and Department of Electrical and Computer Engineering, University of Waterloo, Waterloo, Ontario N2L 3G1, Canada

[§]National Research Council of Canada, Ottawa, Ontario K1A 0R6, Canada

[∥]Department of Applied Physics, Royal Institute of Technology (KTH), AlbaNova University Center, Stockholm SE-106 91, Sweden

S *Supporting Information*

ABSTRACT: Generation of photon pairs from quantum dots with near-unity entanglement fidelity has been a long-standing scientific challenge. It is generally thought that the nuclear spins limit the entanglement fidelity through spin flip dephasing processes. However, this assumption lacks experimental support. Here, we show two-photon entanglement with negligible dephasing from an indium rich single quantum dot comprising a nuclear spin of 9/2 when excited quasi-resonantly. This finding is based on a significantly close match between our entanglement measurements and our model that assumes no dephasing and takes into account the detection system's timing jitter and dark counts. We suggest that neglecting the detection system is responsible for the degradation of the measured entanglement fidelity in the past and not the nuclear spins. Therefore, the key to unity entanglement from quantum dots comprises a resonant excitation scheme and a detection system with ultralow timing jitter and dark counts.

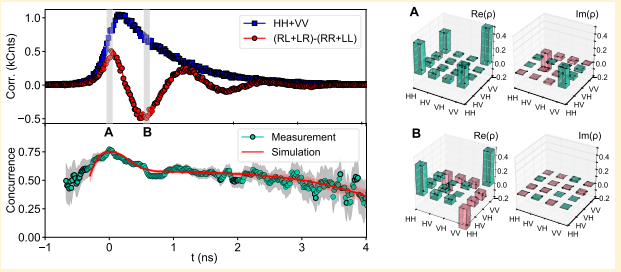

KEYWORDS: *entanglement, fine-structure splitting, quantum dot, single photons*

Quantum dots can generate polarization entangled photons through the biexciton−exciton cascade.[1−3] Understanding how this process can yield perfect polarization entanglement has been a significant scientific challenge for more than a decade. Still, the experimental demonstration of perfect entanglement from quantum dots (QDs) remains elusive.[4,5] The reason is 2-fold. First, QDs must emit perfectly entangled photons, and second, the detection system must be capable of measuring it without degrading its value.[6] Up to now, the detrimental effects of the detection system have been mostly ignored. Nonetheless, they are of equal importance to the photon generation process as timing jitter and dark counts can spoil the measured entanglement. Here, we show that it is possible to reach entanglement with negligible dephasing from QDs by considering both the generation and detection processes of the entangled photons. We construct a model assuming no dephasing and demonstrate a high degree of agreement with our measurements indicating that the investigated quantum dot possesses negligible dephasing. The discovery of dephasing free entanglement generation from a QD makes reaching perfect entanglement in the future merely a technical one.

RESULTS

Dephasing. We start by discussing the physics of how perfect entanglement between the biexciton and the exciton photon can be degraded. Due to the optical selection rules, the spin orientation of the decaying biexciton or exciton electron−hole pair projects onto a certain polarization state. Therefore, we must only analyze how the spins of the biexciton and exciton can loose their spin information. For that, it is crucial to understand that the spin information, responsible for the entanglement generation, can only be destroyed through magnetic fields interacting with the exciton spin. The biexciton remains unaffected as its singlet state does not allow spin flips nor is its energy split through magnetic fields. Thus, we can solely focus our analysis on the exciton with its net one spin. The exciton is influenced by two kinds of magnetic fields. First, nearby spins carried by free or trapped[7] charge carriers or nuclei can lead to an interaction via spin flips. Second, effective magnetic fields caused by electric fields through the spin−orbit coupling can interact with the exciton spin. These electric

Received: October 31, 2018
Published: May 30, 2019

DOI: 10.1021/acsphotonics.8b01496
ACS Photonics 2019, 6, 1656−1663

fields can be decomposed into a static and a time varying contribution. Static fields can reduce the symmetry of the crystal field and are responsible for the so-called fine-structure splitting[8] leading to a precession of the exciton spin.[9,10] Still, this effect is only unitary and leaves the entanglement of the state unaffected, and the possibility of reducing it to approximately zero values ($\simeq$0.1 μeV) has been predicted theoretically as well as shown experimentally.[11−17] However, fluctuating fields from free charge carriers and their spins can lead to dephasing of the quantum state. With a (quasi)-resonant excitation scheme, spin and charge noise from free carriers can be greatly suppressed.[18] Thus, under a (quasi)-resonant excitation scheme, the magnetic field fluctuations from the nuclei should be the only remaining significant source of dephasing. In contrast to assumptions in other works,[4,5,19] we find that this is not a significant source of dephasing and reveal that these interactions are negligible.

In a previous work, it was shown that the nuclear field affects neutral excitons much less than charged exciton complexes.[20] Therefore, the neutral exciton should dephase on an even longer time scale than a charged exciton complex and be negligible during the radiative exciton decay of ~1 ns. This argumentation has been shown to be valid by a study revealing that the neutral exciton spin in InAs quantum dots is not affected by dephasing during the entire radiative lifetime of ~2.5 ns.[21] Remarkably, this result was measured on a system with a large indium content, an element with a significant nuclear spin of 9/2, which has been previously thought to limit dephasing free entanglement.[4,5,19] Furthermore, spin-noise measurements[22] suggest a strong noise suppression at frequencies on the time scale of the exciton lifetime. Our measurements on a wurtzite InAsP quantum dot in a tapered InP nanowire[23] are in good agreement with the above argumentation and reveal that under quasi-resonant excitation the exciton spin does not dephase over the entire exciton decay time of ~5 ns. On the contrary, when excited nonresonantly, the excess charges introduce significant dephasing setting in after ~0.5 ns.

Quasi-Resonant versus Nonresonant Excitation. Figure 1a shows a photoluminescence (PL) spectrum of the QD under study indicating the resonances and the QD s-shell transitions. The peak at 830 nm is the wurtzite InP nanowire band gap transition,[23] and we excited the quantum dot at this wavelength to study the effect of dephasing. In contrast, for the dephasing free measurements, we excited at ~870 nm where there is a manifold of peaks which stem from donor−acceptor transitions and not from the QD's p-shell transitions since these lines were uncorrelated with the QD s-shell transitions.[23,24] Due to the background n-doping ($\approx 1 \times 10^{16}$ cm^{-3}, Supporting Information of ref 25) of the nanowire, the PL spectrum for the two excitation schemes is quite different. In the case of nonresonant excitation, shown in Figure 1b, only three clean peaks from the QD are visible, attributed to the exciton (X), the biexciton (XX), and the negatively charged exciton (X^-). In the case of quasi-resonant excitation (870 nm), Figure 1c, the X^- is suppressed as the quantum dot s-shell is already filled with electrons due to the background n-doping and holes are more mobile, so they can more readily relax into the quantum dot. Here, the positively charged exciton (X^+) dominates the X^- line.

At XX saturation, detected count rates of 940 kCnts/s for the X and 400 kCnts/s for the XX have been recorded with pulsed quasi-resonant excitation at a 76.2 MHz repetition rate

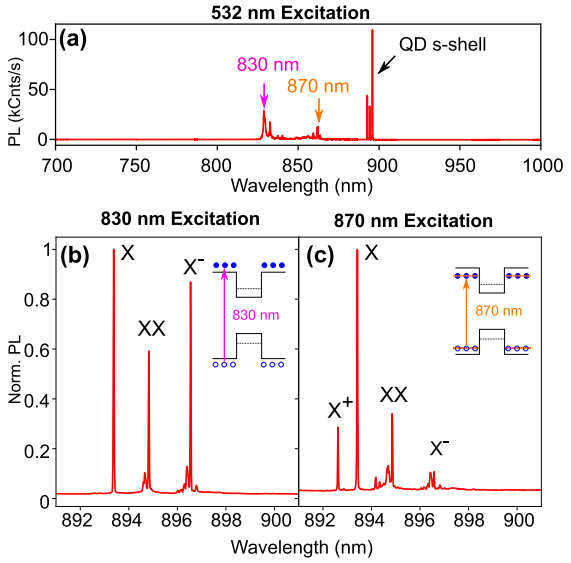

Figure 1. QD emission spectra. (a) Wideband emission spectrum excited with a green laser. For the entanglement measurements, two excitation wavelengths have been used, indicated by an arrow at 830 and 870 nm. (b) Higher resolution spectrum of the QD emission at 830 nm excitation showing three clean peaks attributed to the exciton (X), biexciton (XX), and negatively charged exciton (X^-) at saturation. (c) Increasing the excitation wavelength to 870 nm leads to a different spectrum where X^- is suppressed and the positively charged exciton (X^+) appears. All spectra in panels a−c were recorded at saturation.

and with the quantum state analysis optics removed. The setup efficiency in that case was 6.3% from the first lens until a detected photon. This detected count rate corresponds to a high photon-pair source efficiency of 1.63%, which is 2 orders of magnitude brighter than a quantum dot entangled photon source in the bulk.[26]

In the following, we show that our results exhibit a strong indication of a dephasing free source of entangled photons. This finding suggests that it is possible to reach perfect entanglement from quantum dots, which is in stark contrast to the common understanding[4,5,19] that quantum dots cannot reach "perfect" entanglement due to dephasing mechanisms such as interaction with nuclei. To explain our findings, we use a model of a dephasing free biexciton−exciton cascade. First, we focus on the results of the quasi-resonant excitation scheme and find a close match to the dephasing free model. Second, we compare this quasi-resonant excitation scheme with nonresonant excitation at 830 nm to show the effect of dephasing.

Quasi-Resonant Excitation Matches Dephasing Free Model. The entanglement results of the quasi-resonant excitation scheme are shown in Figure 2 while the comparison between these two excitation schemes will be subsequently discussed. For the biexciton−exciton cascade, we expect to measure a quantum state of the form:[6]

$$|\Psi(t,\delta)\rangle = \frac{1}{\sqrt{2}}(|HH\rangle + e^{-i\frac{\delta}{\hbar}t}|VV\rangle)\Theta(t) \quad (1)$$

where δ represents the fine-structure splitting (FSS) energy, t the time after the biexciton emission, and $\Theta(t)$ the Heaviside step function accounting for the fact that the X photon is created after the XX photon. We denote here the 36 possible correlations within a time interval Δt as N_{ij} with $i, j \in \{H, V, D,$

DOI: 10.1021/acsphotonics.8b01496
ACS Photonics 2019, 6, 1656−1663

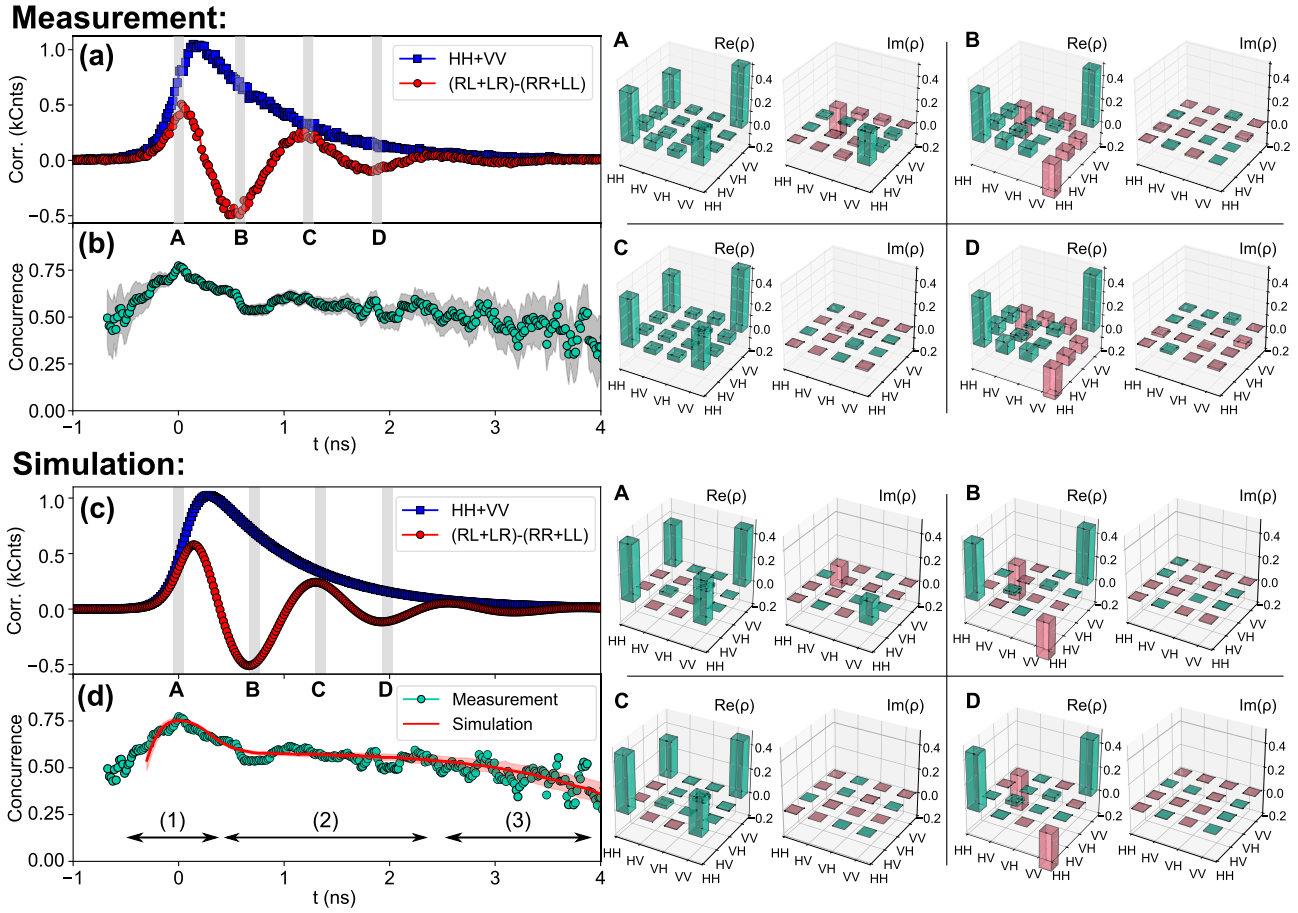

Figure 2. Dephasing free entanglement. (a) Two-photon correlation measurements depicting the sum of the *HH* plus *VV* projections together with $(RL + LR) - (RR + LL)$ showing quantum oscillations. The quantum oscillations appear because the latter term is proportional to the difference of the Bell states $\Phi^+ = 1/\sqrt{2}(|RL\rangle + |LR\rangle)$ and $\Phi^- = 1/\sqrt{2}(|RR\rangle + |LL\rangle)$. The gray shaded areas indicate times with the highest concurrence (A) and times with the smallest imaginary value of the density matrix (B−D). (b) The concurrence extracted from the measurement as a function of time delay, *t*, for all 36 projections. Each data point contains the correlation counts for a Δt = 100 ps time window. The gray area indicates a 2σ concurrence error based on counting statistics. (c) The simulation shows the outcome of a fit free model of the quantum dot, which is in close agreement with the measurement shown in (a). The gray shaded areas indicate times with the highest concurrence (A) and times with the smallest imaginary value of the density matrix (B−D). (d) The concurrence measurement (green solid circles) is superimposed with the simulation (solid red line). The simulation is in very good agreement with the measurement over the entire exciton lifetime, indicating dephasing free entangled photon generation.

$A, R, L\}$ and the measurement polarization projections as H/V (horizontal/vertical), D/A (diagonal/antidiagonal), and R/L (right/left). Here, i and j represent polarization of the X and XX analyzer, respectively. With that, the likelihood p_{ij} of measuring a correlation in the projection $\langle ij|$ within Δt reads as

$$p_{ij} = (|\langle ij|\Psi(t, \delta)\rangle|^2 n(t, \tau_X)) * g(t)\Delta t \quad (2)$$

where $n(t, \tau_X) = 1/\tau_X e^{-t/\tau_X}$ describes the probability of an exciton decay with time constant τ_X, $*$ is the convolution, and $g(t)$ denotes the detector systems' timing resolution function. Therefore, the number of measured correlation counts per time bin becomes $N_{ij} = p_{ij}N_0\Delta t$ where N_0 is the number of collected biexciton−exciton pairs.

On the basis of this mathematical description, the decay of the sum of the correlation counts $HH + VV$ is proportional to the exciton lifetime, τ_X. We plotted the sum of these correlation counts, $HH + VV$, with blue squares in Figure 2a from which we extracted τ_X = 847 ± 6 ps. Furthermore, eq 1 describes an oscillation of the quantum state between the two Bell states $|\Phi^+\rangle = \frac{1}{\sqrt{2}}(|RL\rangle + |LR\rangle)$ and $|\Phi^-\rangle = \frac{1}{\sqrt{2}}(|RR\rangle + |LL\rangle)$ with a period of $\hbar/\delta$. Therefore, plotting the measured correlations $(RL + LR) - (RR + LL)$ reveals quantum oscillations[9,10] between the two Bell states as shown by the red circles in Figure 2a. The quantum oscillation allowed us to accurately measure the FSS to be 795.52 ± 0.35 MHz, an accuracy which is unachievable with typical spectroscopic techniques.[27] We note that the exciton lifetime and FSS completely describe the quantum state evolution as noted in eq 1.

For the entanglement measurements in Figure 2, the QD was excited very close to saturation with an excitation power of 112 nW. The correlations between the X and XX photons were measured in all possible 36 projections[28] $\langle ij|$ instead of the minimal necessary[29] 16. This enabled us to perform a better density matrix reconstruction based on a maximum likelihood approximation.[29,30] We calculated the density matrices using multiple time windows with a width of Δt = 100 ps during the radiative decay of the exciton. Four representative density matrices are shown in the inset of Figure 2. Inset A represents the density matrix at the highest measured concurrence.

DOI: 10.1021/acsphotonics.8b01496
ACS Photonics 2019, 6, 1656−1663

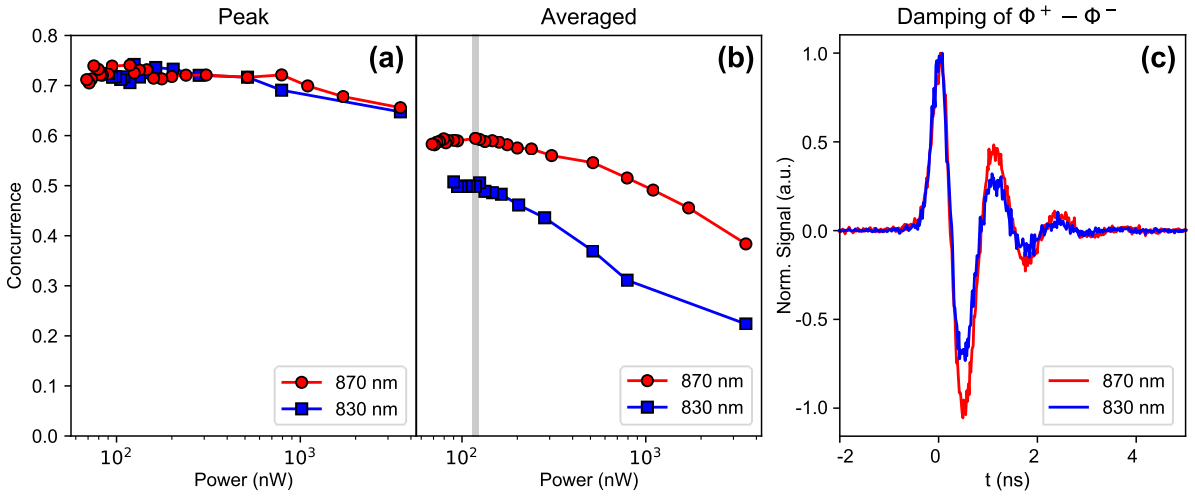

Figure 3. Power dependent entanglement measurements. (a) Peak concurrence calculated on the basis of the two-photon correlation counts measured within a 200 ps wide window for both the quasi- and nonresonant case. There is no significant difference between the case of quasi-resonant excitation (870 nm) and nonresonant excitation (830 nm). (b) Count averaged concurrence over the entire time window for 830 and 870 nm excitation. In this situation, the nonresonant (830 nm) is smaller than the quasi-resonant (870 nm) excitation, highlighting the effect of exciton dephasing. (c) The dephasing can also be visualized directly on the basis of the normalized quantum oscillations when comparing both excitation schemes. The data is taken at the same excitation power as highlighted in gray from panel (b).

Interestingly, there is an imaginary contribution even though eq 1 predicts no imaginary part at $t = 0$. The cause of this effect is the finite timing resolution of the employed avalanche photodiode single photon detectors that averages the phase of the exciton spin precession. In contrast, the density matrices presented in insets B, C, and D were chosen with the smallest imaginary parts. Similarly, the finite detectors' timing resolution is responsible for the smallest imaginary parts not being observed at the extrema of the quantum oscillations but being slightly time delayed.

For a complete picture of the entanglement time evolution, the concurrence $C(\rho)$, defined in ref 31, is a more suitable way of analyzing the entanglement strength of the density matrix ρ. The concurrence scales between zero and one,[31] whereby it is one in the case of the system being fully entangled and zero if the system exhibits only classical correlations. Figure 2b shows the concurrence evolution as a function of time delay where each point was calculated on the basis of the correlations within a $\Delta t = 100$ ps time window. The concurrence reaches a maximum of $C = 0.77 \pm 0.02$, while a counts weighted concurrence average over the whole time window yields $\bar{C} = 0.62 \pm 0.03$.

In Figure 2c,d, we compare the measured result with a simulation assuming a dephasing free QD without any free parameters. Our model, based on eq 2, only considers the finite detection time response, the dark counts, the FSS, the finite $g^{(2)}$ of the XX photon, the detected count rates, and the exciton lifetime that were all determined from the experimentally measured ones. To get a more realistic implementation, we added the detectors' dark counts to the number of correlations of each projection (N_{ij}) before calculating the density matrix ρ_{dc} based on a maximum likelihood approximation. The finite $g^{(2)}_{XX}(0)$ of the biexciton will spoil the entanglement generation in the $g^{(2)}_{XX}(0)$ fraction of the cases. This degrades the entanglement fidelity but is not a source of dephasing. As shown in Figure S1, the power dependent $g^{(2)}$ remains flat at a level of $g^{(2)}(0) = 0.003 \pm 0.003$ for the X and $g^{(2)}(0) = 0.10 \pm 0.01$ for the XX up until the XX saturation point of 640 nW. Therefore, we can add−mix uncorrelated light to ρ_{dc} as

$$\rho_{\mathrm{sim}}(t) = (1 - g^{(2)}_{XX}(0))\rho_{dc}(t) + g^{(2)}_{XX}(0)\frac{\mathbb{1}}{4} \tag{3}$$

where $\rho_{\mathrm{sim}}(t)$ is the result of the simulation, and $\mathbb{1}/4$ is the density matrix for uncorrelated light, $\frac{1}{4}[|HH\rangle\langle HH| + |HV\rangle\langle HV| + |VH\rangle\langle VH| + |VV\rangle\langle VV|]$.

As it can be seen, a high degree of agreement between the model and measurement is achieved without any free parameters. To get a more quantitative number, it is best to compare the correlation counts weighted concurrence average $\bar{C}$ over the full time window. From the simulation, we obtain $\bar{C}(\rho_{\mathrm{sim}}) = 0.61 \pm 0.01$, whereas from the measurement this yields $\bar{C}(\rho) = 0.62 \pm 0.03$. These results agree within their error bounds, further exemplifying their agreement. We therefore conclude that our quantum dot shows negligible dephasing over its entire lifetime.

In addition to the very good agreement of the concurrence, we also see that the density matrices match well between the measurement and the simulation as shown in the insets of A−D. Of particular interest is inset A. Both the simulation and the measurement exhibit nonvanishing imaginary parts. The reason for this observation is phase averaging during the exciton precession caused by the finite timing resolution of the detectors. This effect has been seen before,[10] but a convincing explanation has remained elusive.

Another supporting fact is the close to perfect agreement of the concurrence simulation with the concurrence extracted from the measurement depicted in Figure 2d. Here, we identify three regimes: (1) the "top" part; (2) the "flat" part; (3) "roll-off" part. The "top" part exhibits a concurrence maximum because the concurrence first rises as the detector response function $g(t)$ samples more and more correlation counts with evolving time, t. At a certain level, however, the phase averaging of the exponential term in eq 1 dominates and the concurrence falls. Once the whole $g(t)$ function samples the state evolution, the phase averaging remains constant, named the "flat" part. With evolving time, less correlations are measured due to the exponential decay of the X photon, which

DOI: 10.1021/acsphotonics.8b01496
ACS Photonics 2019, 6, 1656−1663

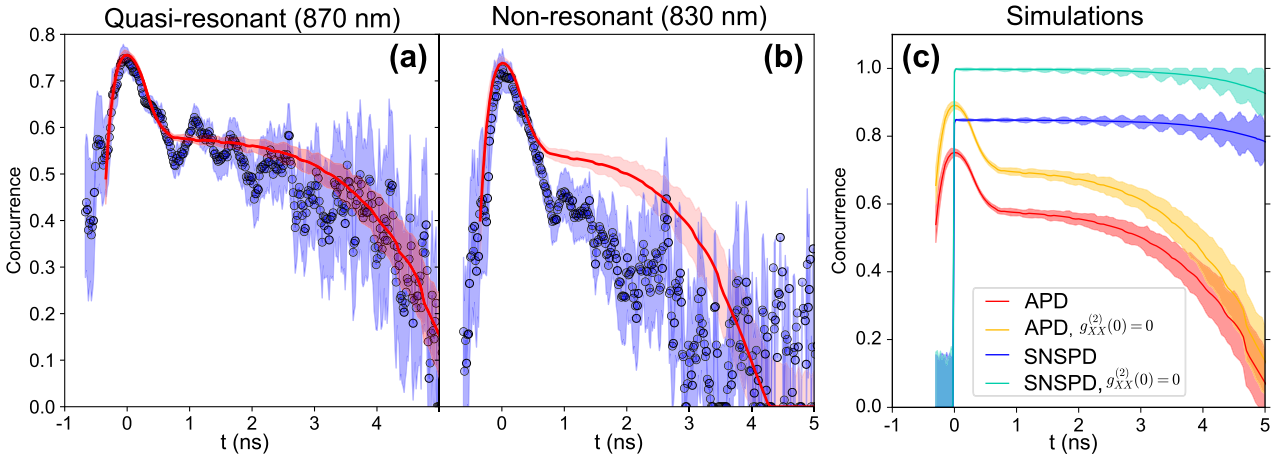

Figure 4. Toward near-unity entanglement: comparison of dephasing and dephasing free entanglement. (a) At quasi-resonant excitation, the measured concurrence evolution agrees with the simulation within error bars, thus signifying dephasing free entanglement. (b) At nonresonant excitation, the measured concurrence evolution does not match with the simulation indicating dephasing. The data in both (a) and (b) was taken from the two points highlighted in the gray region of Figure 3b. (c) Four simulation curves illustrating the effect of finite detection time resolution and multiphoton emission of the biexciton photon. The red graph depicts the same simulation as already presented in Figure 2d with finite $g^{(2)}_{XX}$ = 0.1 and the yellow graph is the case for zero $g^{(2)}_{XX}$ = 0 in both cases for a slow detection system based on an avalanche photodiode single-photon detector (APD) as a reference. The blue curve shows the outcome of a simulation similar to the red curve with finite $g^{(2)}_{XX}$ = 0.1 but with a fast detection system based on a superconducting nanowire single photon detector (SNSPD) with 30 ps timing resolution. The cyan curve is the same as the blue curve with SNSPD but for pure single photon emission of the biexciton photon (i.e., with $g^{(2)}_{XX}(0) = 0$). Remarkably, with a fast detection system and perfect $g^{(2)}_{XX}$, near-unity entanglement is expected. Dark counts used in the simulation for the APDs are 36.3 and 18.2 s^{-1} for the *X* and *XX* detector, respectively, and for the SNSPDs are 1 s^{-1}.

is when we enter the "roll-off" part where the concurrence drops due to the detectors' dark counts. It is important to note that the whole entanglement evolution with its three parts can be completely described without any dephasing from the QD. The three regimes are solely caused by the finite timing resolution and dark counts from the detection system.

Nonresonant Excitation Induces Dephasing. We now repeat the experiment with nonresonant excitation and compare it with the quasi-resonant excitation scheme. Figure 3a depicts the peak concurrence for the two different excitation schemes as a function of excitation power. Each data point is constructed by analyzing the correlation counts within a Δt = 200 ps time window centered at t = 0. The integration window is increased here to better cope with count differences in the power dependent measurements spanning more than a decade but does not otherwise influence the outcome of the analysis. The result reveals that both excitation schemes provide the same power dependent peak concurrence measurement. The cause for the concurrence to drop at higher excitation power is the increase of the biexciton $g^{(2)}$ value, which is not a dephasing effect. The situation is quite different when we compare the correlation weighted concurrence average over the full time window as presented in Figure 3b. Clearly, the data for 830 nm excitation shows ∼15% smaller concurrence as compared to the quasi-resonant case at low powers, while deviating further at higher powers. This result is expected from the excess charges generated by nonresonant excitation. First, the spin of these charges can cause direct spin flip−flop processes with the exciton spin. Second, fluctuating electric fields caused by the excess charges can result in an effective magnetic field via the spin−orbit interaction and alter the exciton spin. This situation is directly visible in Figure 3c where the normalized quantum oscillations are compared with each other. The two curves were recorded at the same power level highlighted by the shaded region in Figure 3b. The 830 nm data clearly damps out faster than the 870 nm one, which is the fingerprint for dephasing.

To show the dephasing effect more quantitatively, we simulated the two cases as presented in Figure 4. Please note that the results in Figure 4a,b were recorded at the same excitation power (118 nW) indicated with the gray bar in Figure 3b whereas the data in Figure 2a was recorded at a slightly lower power (112 nW). Again, the model in Figure 4a agrees with the quasi-resonant excitation scheme within error bars indicative for dephasing free entanglement. In contrast, the situation is very different for nonresonant excitation (Figure 4b) where the simulation clearly overestimates the measurement exemplifying dephasing.

Influence of the Detection System. Finally, we investigate what the concurrence evolution of the data presented in Figure 2 would look like if we were to measure with an emerging detection system employing a better timing resolution and lower dark count rate. We assume a timing resolution of 30 ps full width at half-maximum and a dark count rate of 1 Hz, values which can be met by recently available superconducting nanowire single photon detectors. The outcome of such simulations are plotted in Figure 4c for $g^{(2)}_{XX}(0)$ = 0 and $g^{(2)}_{XX}(0)$ = 0.1 and are compared to the case when measuring with our APDs in the situation of zero or finite $g^{(2)}_{XX}(0)$ = 0.1 (i.e., with the same plot as in Figure 2d). With APDs, we get a peak concurrence of $C = 0.75 \pm 0.01$ at finite $g^{(2)}_{XX}(0)$, and in case of zero $g^{(2)}_{XX}(0)$, the simulation predicts that we would measure a peak concurrence of $C = 0.89 \pm 0.01$ but maintain the overall shape of the concurrence evolution. In both cases with 30 ps timing resolution, i.e., with zero $g^{(2)}_{XX}(0)$ and finite $g^{(2)}_{XX}(0)$, the difference to the simulation with APDs is quite striking. First, the peak concurrence for finite $g^{(2)}_{XX}(0)$ = 0.1 ($C = 0.849 \pm 0.001$)) and $g^{(2)}_{XX}(0)$ = 0 ($C = 0.999 \pm 0.001$) is significantly larger than for the case of measuring with APDs

DOI: 10.1021/acsphotonics.8b01496
ACS Photonics 2019, 6, 1656−1663

and finite $g^{(2)}_{XX}(0)$. Remarkably, the concurrence reaches near-unity for zero $g^{(2)}(0)$. Second, the shapes of the curves have changed significantly. The "top" part is completely suppressed. Instead, only the "flat" and "roll-off" parts remain. It is interesting to note that even the small dark count rate of 1 Hz is inducing a resolvable entanglement roll-off. However, this decrease at the end has a minimal effect on the overall concurrence, and count averaged concurrences of $\overline{C} = 0.996^{+0.004}_{-0.008}$ for zero $g^{(2)}_{XX}(0)$ and $\overline{C} = 0.847 \pm 0.007$ in the case of finite $g^{(2)}_{XX}(0)$ are obtained. The slight oscillations visible in the concurrence's error for the high temporal resolution simulation are not artifacts. They are caused by counting statistics since every time one of the 36 simulated correlations reaches zero the concurrence can be less accurately estimated. This happens with a frequency four times larger than the FSS. In fact, this effect is visible in other groups' measurements, for example, in the fidelity evolution of ref 9. For a slower detection system, such as our APDs, this effect is averaged out.

DISCUSSION

We have shown that our model is capable of explaining our measurement results in great detail. The question arises: why has dephasing free entanglement from QDs not been observed before? The reason is that a QD with a long X decay time of $\tau_X \sim 1$ ns is needed in conjunction with a (quasi)-resonant excitation scheme. For example, in refs 4 and 18, a resonant excitation scheme was employed, but the QDs had a τ_X of ~200 ps, which makes it very difficult to separate the detrimental effects from the detection system. However, on the basis of model calculations, we predict that the QDs investigated in these aforementioned works of refs 4 and 18 should also be dephasing free. Therefore, the occurrence of dephasing free entanglement is not at all limited to InAsP QDs but should be equally achievable in other QD materials such as InGaAs[18] and GaAs.[4]

Even though our results suggest the existence of dephasing free entanglement, we have not yet shown unity concurrence. The reduction of the measured concurrence from unity comes mainly from the detectors' timing resolution, finite $g^{(2)}_{XX}$ value of the QD, and dark counts. Still, $g^{(2)}$ values of both the exciton and biexciton can be brought to zero by resonant excitation.[4,18,32] Therefore, in principle, the problem of reaching perfect entanglement using QDs should now be merely a technical one, which in future work, can be resolved by combining the right source and excitation scheme with a state-of-the-art detection system. However, there are always challenges regarding the re-excitation of the s-shell,[33] which may be addressed by using proper protocols.[34−36]

CONCLUSION

We have established a precise model of the entanglement measurement in which the generation and the detection processes of entangled photon pairs are of equal importance. On the basis of this knowledge, we could show that a QD containing indium generates photon entanglement with negligible dephasing over the entire exciton decay time even though it has a large nuclear spin of 9/2. This result is remarkable as it indicates that perfect entanglement is achievable in QDs in spite of the interaction with nuclei possessing large nuclear spins. The conditions needed to resolve dephasing free entanglement are (quasi)-resonant excitation and a precise knowledge of the employed detection system. This new insight will allow one to make an ideal entangled photon source based on QDs. On the basis of our model, we suggest that dephasing free entanglement should also be found in materials other than InAsP, such as InGaAs[18] and GaAs[4] QDs. However, the actual evidence can be presented once the resonant excitation schemes, as well as the fast detectors with low dark counts, are used to repeat the measurements.

METHODS

Quantum Dot. The quantum dot growth is described in the Methods Section of ref 27.

Measurement. We used a standard micro-PL setup where the nanowire sample was kept at a base temperature of 4.5 K. The light from a picosecond pulsed laser was filtered with a 1200 lines/mm grating to reduce the effect of laser background fluorescence before it was used to excite the QD. For the quantum state tomography, we used a similar system as in ref 26; the difference was that the waveplates were mounted in high-precision motorized mounts crucial for the repeatability of the experiment. The first beam splitter used to excite the QD had 30% reflection and 70% transmission. The excitation was performed in all cases with s-polarized light to prevent nuclear polarization.[37] All correlation data was sampled with 16 ps resolution.

The data presented in Figure 2 was excited with a power of 112 nW and integrated for 370 s per projection. Count rates were in an *HH* projection of 71 kCnt/s for the X and 8 kCnts/s for the XX. The data presented in Figure 4a,b was excited with a power of 118 nW and integrated for 342 s per projection. In the case of Figure 4a, this resulted in an *HH* projection count rate of 85 kCnt/s for the X and 11 kCnts/s for the XX, and for Figure 4b, it was an *HH* projection count rate of 73 kCnt/s for the X and 4.4 kCnts/s for the XX.

The employed avalanche single-photon detectors (APDs) had a dark count rate of 36.3 s^{-1} for the detector measuring the exciton and 18.2 s^{-1} for the biexciton detector with a time resolution of 290 ps full width at half-maximum; see Figure S10.

Simulation. For the simulation in the text, we used an FSS of 795.520 MHz, a dark count rate of 36.3 s^{-1} for the exciton and 18.2 s^{-1} for the biexciton detector, an exciton lifetime (τ_X) of 847 ps, a $g^{(2)}_{XX}$ of 0.1, a $g^{(2)}_{X}$ of 0, and a laser repetition rate of 76.2 MHz. The used count rates and integration times are stated in the Measurement section. In the case of Figure 2b, an exciton lifetime of τ_X = 753 ps was used.

The density matrix reconstruction was performed on the basis of the code from ref 30. The method of how to acquire the system's timing resolution $g(t)$ is described in the Supporting Information.

The error of the concurrence is estimated on the basis of a Monte Carlo simulation assuming counting statistics. For each concurrence value, the simulation was performed with 1000 repetitions.

ASSOCIATED CONTENT

Supporting Information

The Supporting Information is available free of charge on the ACS Publications website at DOI: 10.1021/acsphotonics.8b01496.

DOI: 10.1021/acsphotonics.8b01496
ACS Photonics 2019, 6, 1656−1663

Power dependence of exciton and biexciton; quantum dot characteristics; tomography setup calibration; correlation measurements; birefringence; detector time resolution function; count averaged concurrence (PDF)

AUTHOR INFORMATION

Corresponding Author

*E-mail: arash.ahmadi@uwaterloo.ca.

ORCID

A. Fognini: 0000-0002-2895-1110

A. Ahmadi: 0000-0002-8115-5324

K. D. Jöns: 0000-0002-5814-7510

Author Contributions

⊥A.F. and A.A. contributed equally to this work.

Notes

The authors declare no competing financial interest.

The authors declare that the main data supporting the findings of this study are available within the Article and its Supporting Information. The used quantum tomography code[30] is available at https://github.com/afognini/Tomography.

ACKNOWLEDGMENTS

A.F. gratefully acknowledges the Swiss National Science Foundation for the support through their Early PostDoc Mobility Program. M.E.R. acknowledges Industry Canada and NSERC for support. K.D.J. acknowledges funding from the Marie Skłodowska Individual Fellowship under REA grant agreement No. 661416 (SiPhoN) and the Kungliga Vetenskapsakademien Physics 2016 scholarship.

REFERENCES

(1) Benson, O.; Santori, C.; Pelton, M.; Yamamoto, Y. Regulated and Entangled Photons from a Single Quantum Dot. *Phys. Rev. Lett.* **2000**, *84*, 2513−2516.

(2) Hafenbrak, R.; Ulrich, S. M.; Michler, P.; Wang, L.; Rastelli, A.; Schmidt, O. G. Triggered polarization-entangled photon pairs from a single quantum dot up to 30 K. *New J. Phys.* **2007**, *9*, 315.

(3) Salter, C. L.; Stevenson, R. M.; Farrer, I.; Nicoll, C. A.; Ritchie, D. A.; Shields, A. J. An entangled-light-emitting diode. *Nature* **2010**, *465*, 594−597.

(4) Huber, D.; Reindl, M.; Huo, Y.; Huang, H.; Wildmann, J. S.; Schmidt, O. G.; Rastelli, A.; Trotta, R. Highly indistinguishable and strongly entangled photons from symmetric GaAs quantum dots. *Nat. Commun.* **2017**, *8*, 15506.

(5) Keil, R.; Zopf, M.; Chen, Y.; Höfer, B.; Zhang, J.; Ding, F.; Schmidt, O. G. Solid-state ensemble of highly entangled photon sources at rubidium atomic transitions. *Nat. Commun.* **2017**, *8*, 15501.

(6) Stevenson, R. M.; Hudson, A. J.; Bennett, A. J.; Young, R. J.; Nicoll, C. A.; Ritchie, D. A.; Shields, A. J. Evolution of Entanglement Between Distinguishable Light States. *Phys. Rev. Lett.* **2008**, *101*, 170501.

(7) Witzel, W. M.; Carroll, M. S.; Morello, A.; Cywiński, L.; Das Sarma, S. Electron Spin Decoherence in Isotope-Enriched Silicon. *Phys. Rev. Lett.* **2010**, *105*, 187602.

(8) Singh, R.; Bester, G. Nanowire Quantum Dots as an Ideal Source of Entangled Photon Pairs. *Phys. Rev. Lett.* **2009**, *103*, 063601.

(9) Ward, M.; Dean, M.; Stevenson, R.; Bennett, A.; Ellis, D.; Cooper, K.; Farrer, I.; Nicoll, C.; Ritchie, D.; Shields, A. Coherent dynamics of a telecom-wavelength entangled photon source. *Nat. Commun.* **2014**, *5*, 3316.

(10) Huber, T.; Predojević, A.; Khoshnegar, M.; Dalacu, D.; Poole, P. J.; Majedi, H.; Weihs, G. Polarization Entangled Photons from Quantum Dots Embedded in Nanowires. *Nano Lett.* **2014**, *14*, 7107−7114.

(11) Wang, J.; Gong, M.; Guo, G.-C.; He, L. Eliminating the fine structure splitting of excitons in self-assembled InAs/GaAs quantum dots via combined stresses. *Appl. Phys. Lett.* **2012**, *101*, 063114.

(12) Huber, D.; Reindl, M.; Filipe, S.; Schimpf, C.; Martín-sánchez, J.; Huang, H.; Piredda, G.; Edlinger, J.; Rastelli, A.; Trotta, R. Strain-Tunable GaAs Quantum Dot: A Nearly Dephasing-Free Source of Entangled Photon Pairs on Demand. *Phys. Rev. Lett.* **2018**, *121*, 33902.

(13) Zeeshan, M.; Sherlekar, N.; Ahmadi, A.; Williams, R. L.; Reimer, M. E. Quadrupole electric field for erasing the fine structure splitting in a single quantum dot. 2018, arXiv:1809.02538. arXIV.org e-Print archive. http://arxiv.org/abs/1809.02538.

(14) Fognini, A.; Ahmadi, A.; Daley, S. J.; Reimer, M. E.; Zwiller, V. Universal fine-structure eraser for quantum dots. *Opt. Express* **2018**, *26*, 24487−24496.

(15) Jones, N. S.; Stace, T. M. Photon frequency-mode matching using acousto-optic frequency beam splitters. *Phys. Rev. A: At., Mol., Opt. Phys.* **2006**, *73*, 033813.

(16) Trotta, R.; Martín-Sánchez, J.; Wildmann, J. S.; Piredda, G.; Reindl, M.; Schimpf, C.; Zallo, E.; Stroj, S.; Edlinger, J.; Rastelli, A. Wavelength-tunable sources of entangled photons interfaced with atomic vapours. *Nat. Commun.* **2016**, *7*, 10375.

(17) Trotta, R.; Zallo, E.; Ortix, C.; Atkinson, P.; Plumhof, J.; Van den Brink, J.; Rastelli, A.; Schmidt, O. Universal recovery of the energy-level degeneracy of bright excitons in InGaAs quantum dots without a structure symmetry. *Phys. Rev. Lett.* **2012**, *109*, 147401.

(18) Müller, M.; Bounouar, S.; Jöns, K. D.; Glässl, M.; Michler, P. On-demand generation of indistinguishable polarization-entangled photon pairs. *Nat. Photonics* **2014**, *8*, 224−228.

(19) Kuroda, T.; Mano, T.; Ha, N.; Nakajima, H.; Kumano, H.; Urbaszek, B.; Jo, M.; Abbarchi, M.; Sakuma, Y.; Sakoda, K.; Suemune, I.; Marie, X.; Amand, T. Symmetric quantum dots as efficient sources of highly entangled photons: Violation of Bell's inequality without spectral and temporal filtering. *Phys. Rev. B: Condens. Matter Mater. Phys.* **2013**, *88*, 041306.

(20) Urbaszek, B.; Marie, X.; Amand, T.; Krebs, O.; Voisin, P.; Maletinsky, P.; Högele, A.; Imamoglu, A. Nuclear spin physics in quantum dots: An optical investigation. *Rev. Mod. Phys.* **2013**, *85*, 79−133.

(21) Sénés, M.; Liu, B. L.; Marie, X.; Amand, T.; Gérard, J. M. In *Optical Properties of 2D Systems with Interacting Electrons*; Ossau, W. J., Suris, R., Eds.; Springer Netherlands: Dordrecht, 2003; pp 79−88.

(22) Kuhlmann, A. V.; Houel, J.; Ludwig, A.; Greuter, L.; Reuter, D.; Wieck, A. D.; Poggio, M.; Warburton, R. J. Charge noise and spin noise in a semiconductor quantum device. *Nat. Phys.* **2013**, *9*, 570−575.

(23) Dalacu, D.; Mnaymneh, K.; Lapointe, J.; Wu, X.; Poole, P. J.; Bulgarini, G.; Zwiller, V.; Reimer, M. E. Ultraclean Emission from InAsP Quantum Dots in Defect-Free Wurtzite InP Nanowires. *Nano Lett.* **2012**, *12*, 5919−5923.

(24) Gadret, E. G.; Dias, G. O.; Dacal, L. C.; De Lima, M. M.; Ruffo, C. V.; Iikawa, F.; Brasil, M. J.; Chiaramonte, T.; Cotta, M. A.; Tizei, L. H.; Ugarte, D.; Cantarero, A. Valence-band splitting energies in wurtzite InP nanowires: Photoluminescence spectroscopy and ab initio calculations. *Phys. Rev. B: Condens. Matter Mater. Phys.* **2010**, *82*, 1−5.

(25) Reimer, M. E.; Bulgarini, G.; Fognini, A.; Heeres, R. W.; Witek, B. J.; Versteegh, M. A. M.; Rubino, A.; Braun, T.; Kamp, M.; Höfling, S.; Dalacu, D.; Lapointe, J.; Poole, P. J.; Zwiller, V. Overcoming power broadening of the quantum dot emission in a pure wurtzite nanowire. *Phys. Rev. B: Condens. Matter Mater. Phys.* **2016**, *93*, 195316.

(26) Jöns, K. D.; Schweickert, L.; Versteegh, M. A. M.; Dalacu, D.; Poole, P. J.; Gulinatti, A.; Giudice, A.; Zwiller, V.; Reimer, M. E. Bright nanoscale source of deterministic entangled photon pairs violating Bell's inequality. *Sci. Rep.* **2017**, *7*, 1700.

(27) Versteegh, M. A. M.; Reimer, M. E.; Jöns, K. D.; Dalacu, D.; Poole, P. J.; Gulinatti, A.; Giudice, A.; Zwiller, V. Observation of

DOI: 10.1021/acsphotonics.8b01496
ACS Photonics 2019, 6, 1656−1663

strongly entangled photon pairs from a nanowire quantum dot. *Nat. Commun.* **2014**, *5*, 5298.
(28) de Burgh, M. D.; Langford, N. K.; Doherty, A. C.; Gilchrist, A. Choice of measurement sets in qubit tomography. *Phys. Rev. A: At., Mol., Opt. Phys.* **2008**, *78*, 052122.
(29) James, D. F. V.; Kwiat, P. G.; Munro, W. J.; White, A. G. Measurement of qubits. *Phys. Rev. A: At., Mol., Opt. Phys.* **2001**, *64*, 052312.
(30) Fokkens, T.; Fognini, A.; Zwiller, V. *Optical Quantum Tomography Code*; 2016−2017; Available at https://github.com/afognini/Tomography.
(31) Wootters, W. K. Entanglement of Formation of an Arbitrary State of Two Qubits. *Phys. Rev. Lett.* **1998**, *80*, 2245−2248.
(32) Somaschi, N.; et al. Near-optimal single-photon sources in the solid state. *Nat. Photonics* **2016**, *10*, 340−345.
(33) Fischer, K. A.; Hanschke, L.; Wierzbowski, J.; Simmet, T.; Dory, C.; Finley, J. J.; Vučković, J.; Müller, K. Signatures of two-photon pulses from a quantum two-level system. *Nat. Phys.* **2017**, *13*, 649.
(34) Schweickert, L.; Jöns, K. D.; Zeuner, K. D.; Covre Da Silva, S. F.; Huang, H.; Lettner, T.; Reindl, M.; Zichi, J.; Trotta, R.; Rastelli, A.; Zwiller, V. On-demand generation of background-free single photons from a solid-state source. *Appl. Phys. Lett.* **2018**, *112*, 093106.
(35) Wei, Y. J.; He, Y. M.; Chen, M. C.; Hu, Y. N.; He, Y.; Wu, D.; Schneider, C.; Kamp, M.; Höfling, S.; Lu, C. Y.; Pan, J. W. Deterministic and robust generation of single photons from a single quantum dot with 99.5% indistinguishability using adiabatic rapid passage. *Nano Lett.* **2014**, *14*, 6515−6519.
(36) Hanschke, L.; Fischer, K. A.; Appel, S.; Lukin, D.; Wierzbowski, J.; Sun, S.; Trivedi, R.; Vuckovic, J.; Finley, J. J.; Müller, K. Quantum dot single-photon sources with ultra-low multi-photon probability. *npj Quantum Information* **2018**, *4*, 43.
(37) Belhadj, T.; Kuroda, T.; Simon, C.-M.; Amand, T.; Mano, T.; Sakoda, K.; Koguchi, N.; Marie, X.; Urbaszek, B. Optically monitored nuclear spin dynamics in individual GaAs quantum dots grown by droplet epitaxy. *Phys. Rev. B: Condens. Matter Mater. Phys.* **2008**, *78*, 205325.

DOI: 10.1021/acsphotonics.8b01496
ACS Photonics 2019, 6, 1656−1663